Available online at www.sciencedirect.com

SciVerse ScienceDirect

Procedia Environmental Sciences 11 (2011) 1513 – 1521

Procedia Environmental Sciences

Influence of different cover ratios on Gas-particle flow characteristics of a centrally-fuel-rich primary air burner: experiment and simulation

Zhichao Chen, Shanping Shen, Zhengqi Li, Qunyi Zhu

School of Energy Science and Engineering,Harbin Institute of Technology, 92, West Dazhi Street, Harbin150001, China
e-mail: chenzc@hit.edu.cn

Abstract

The flow field for different cover ratios within a three-level conical ring concentrator of a centrally-fuel-rich swirl coal combustion burner has been studied both experimentally and numerically. A particle dynamics anemometer measurement system was employed in the study to measure velocity and particle volume flux after the outlet of third-level ring. And the numerical simulations were used to calculate the flow field in the conical ring region. In each cross-section, after the outlet of third-level ring, concentration ratio for each cover ratio is always larger than 2. With conical ring concentrator in the primary air tube, the coal concentration can be concentrated to a suitable range. In the cross-sections $0.5<x/D<4.0$, as cover ratio increases, concentration ratio decreases and resistance coefficient increases.

Keywords: Gas/particle flow; PDA; Concentrator; Numerical simulation;

1. Introduction

Coal is the most abundant fossil fuel around the world and many countries use coal as fuel for power plant [1, 2]. The coal combustion can cause serious air pollution [3-5], such as NOx, SOx, CO_2 and so on. To lessen environmental pollution, the allowed NOx emission from power plants has been lowered in many countries. In China for example, The pulverized coal power generation units built after 2004 should have NOx levels under 450 mg/Nm^3 at 6% O_2 (dry basis) when burning coals with more than 20% volatiles (dry ash-free basis) [6]. To meet the requirement of environmental protection, many kinds of lower NOx-emission techniques were developed. The low NOx swirl burners are almost designed for high grade coal, which have the high sensitivity to the type of coal. In China, most of coal used in power plants is low grade coal with low calorific value, low volatility and low ash fusion temperature. When burning low-grade coal, it is difficult for low-NOx burners that are designed to burn high-grade coal to meet power industry requirements such as flame stability and no slagging propensity.

To burn low-grade coal, many types of pulverized coal concentrators, such as the louver type and collision-block type, have been developed and investigated [7]. Increasing the pulverized coal concentration within a defined range can increase the combustion rate and decrease NO formation. W. D. Fan investigated the combustion characteristics of fuel-rich jet combustion technology and concluded that fuel-rich and fuel-lean flow can realize stable-flame combustion, low NOx emissions, and slagging prevention [8]. Experiments [9–11] have shown that fuel-rich and fuel-lean combustion not only improves ignition, flame velocity and burnout of low-volatility coal but may also reduce NOx emissions. For low-volatility coals, the fuel/air mass ratio needs to be within the range of 0.6–1.4 kg (coal)/kg (air) to achieve stable ignition, which is twice the fuel/air mass ratio at the entrance of the primary air duct [12]. Calculation results for swirling pulverized-coal combustion obtained similar results [13, 14]. W. D. Fan et al. [15–16] measured gas/solid flows in a louver coal

doi:10.1016/j.proenv.2011.12.228

concentrator, predicted the abrasion of blades by numerical simulation and draw a conclusion that the structure parameters is important for the performance of the concentrator.

Prof. Li, et al. proposed the centrally fuel-rich swirl coal combustion burner in 2003 [17–22]. Conical rings are taken as the concentrator for CFR burner. The burner has wide applications in 670t/h and 1025t/h boilers burning bituminous coal and low quality coal. Boilers fitted with these CFR burners demonstrated improved combustion stability and capacity at low load, better boiler efficiency, and lowered NOx emissions with high coal adaptability. Moreover, slagging and high-temperature corrosion did not occur [17, 18, 21]. Conical rings are a key component for CFR burner. In previous studies on CFR burners [18, 20, 22], a fuel-rich duct was installed in the model burner to substitute for conical ring concentrator. The effect of conical ring concentrator on the primary air was not studied. In this paper, influence of different cover ratios on gas-particle flow characteristics downstream from the third-level ring of the concentrator were studied using a particle dynamics anemometer (PDA) system and measured cases with cover ratio 0, 0.375 and 0.5. As the gap between the rings is too narrow, experiments can not measure the conical ring region. The flow fields in the conical ring region were studied by numerical simulation and calculated cases with cover ratio 0, 0.2, 0.375 and 0.5, respectively.

2. Experimental system

The test facility used in this investigation is illustrated schematically in Fig. 1, included a suction device, feeder, particle reservoir, test pipe and cyclone separator. Air flow was induced in the pipe by the suction device, the inlet velocity of primary air being 16.7m/s. Since coal particles cannot meet the steradian and reflectance characteristics required for PDA particle measurements, glass beads, which do meet these requirements, were used instead. Glass beads, of density 2500 kg/m^3 and mean diameter 42 μm, were use to represent coal particles and were fed via the feeder into the head of the test section, measuring 2,400mm in length and having glass window monitoring ports to allow access for velocity measurements. For this purpose, this investigation employed a PDA system made by Dantec Dynamics Company. The gas/particle mixture flowed through a bag-type dust collector and then a cyclone collector from where collected particles were fed into the particle reservoir. After each experiment, the glass windows were removed for cleaning.

The conical rings, arranged in three concentric levels according to diameter, are installed in the primary air duct of concentrator (see Fig. 2). Its main parameters are as follows: the diameter of the primary air duct (D) is 140mm, the exit diameter of the third–level ring (d) is 70mm, the distance between adjacent rings (L) is 32mm, and other parameters include x as the axial distance between measuring points and the outlet of the third–level ring and r as the radial distance between measuring points and the axis, the origin for both x and r was located at the center of the outlet of third-level ring. All axial distances are given as reduced distances x/D. The definition of the cover ratio of the conical ring is as follows:

$$w=p/b\sin\alpha \tag{1}$$

Where p is the cover height of conical ring, α is the angle of conical ring and b is the width of conical ring.

The particle mass concentration fraction is 0.1kg/kg, and refers to the specific value of mass concentration of glass beads and mass concentration of airflow in the primary. Velocities at eight cross–sections downstream from the third-level ring were measured using the PDA system. Measurements were taken mainly in the vicinity of the axis of the concentrator with 3000 samples taken at each point. Particles with diameters of 0–8 μm were used to trace the air flow and particles with diameters of 10–100 μm were used to represent the particle phase flow.

3. Numerical simulation method

3.1. Mathematical models

FLUENT 6.3.26 software was used to calculate, in particular, flow fields using a range of widely–used numerical models. The calculation procedure includes numerical solution of the time–averaged conservation equations for the gas and particle phases, using the Eulerian description for the gas phase and lagrangian description for the particle phase. Gas turbulence was specifically taken into account by the so–called realizable k–ε model [23]. The Lagrangian stochastic tracking model was applied to analyze the gas/particle flow field [24], while calculations of gas/particle two–phase coupling employed the particle–source–in–cell method. Using the finite difference method to discretize differential equations, the governing equation was solved using the SIMPLEC algorithm and first–order upwind differencing scheme. The duct inlet boundary conditions are assumed to have uniform distributions and are based on modeling data. The inlet conditions define as uniform inflow velocity by specifying the velocity magnitude normal to the inlet. For the turbulence inlet condition, the turbulence intensity is 10% and the hydraulic diameter is 0.14m. The outlet conditions are the fully developed solutions to the governing equations, which are expressible in the form:

$$\frac{\partial \phi}{\partial z} = 0, \quad \phi = u, \quad v, \quad w, \quad p, \quad k, \quad \varepsilon \tag{2}$$

Wall boundary conditions assume no slip and no turbulence and take the form:

$$\vec{u}\big|_w = 0, \quad \vec{v}\big|_w = 0, \quad \vec{w}\big|_w = 0, \quad p\big|_w = 0, \quad k\big|_w = 0, \quad \varepsilon\big|_w = 0 \tag{3}$$

3.2. Computational domain specifications and calculated parameters

The geometric model of the concentrator used in the simulations is two dimensions. Fig. 3 shows schematic diagram of grid divisions throughout the computational domain of the concentrator. This domain is divided into a steady inlet region, a concentrator region and an outlet region. A refined grid was constructed within those regions of maximum interest where sudden changes in fluid flow are expected; for example, in the conical ring region and the outlet region (see Fig. 3). Over the computational domain, grids were chosen to ensure as far as possible that flow is normal to the grids, so as "false diffusion" does not arise. For the steady inlet region, a quadrilateral–structured grid is used with grid aspect ratio of 1:3. In the concentrator region, an adaptive quadrilateral grid is used. The outlet region is quadrilateral–structured grids with grid aspect ratio of 1:1.

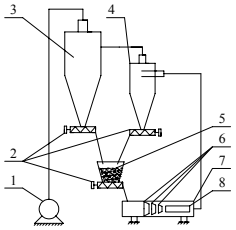

1. Suction device 2. Feeder 3. Bag house dust collector 4. Cyclone separator 5. Particle reservoir 6. Pulverized coal concentration rings 7. Test section 8. Measurement window

Figure 1. Schematic diagram of the test facility

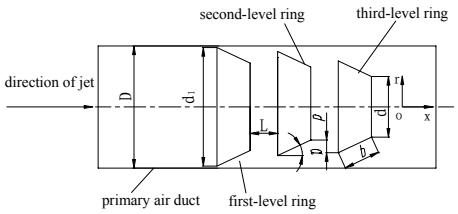

Figure 2. Schematic diagram of the conical concentrator with three levels of rings.

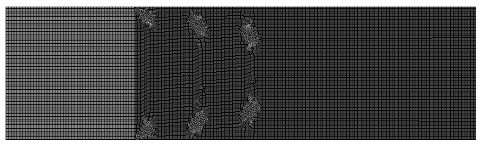

Figure 3. Schematic diagram of grid divisions of the computational domain for a three–level conical ring concentrator.

4. Results and discussion

4.1. Axial velocities (By experiments)

Fig. 4 shows profiles of the gas/particle mean axial velocities for three *w*. In four cross–sections from *x*/*D*=0.1 to 1.0, it can be seen that the profiles have one peak and one valley. The peaks values appears at the radial position *r*=35mm, which is the radius of the exit of the third - level ring. Gas/particle mixture is concentrated, after flowing through the three levels conical ring. In all cross–sections, in the radius range from 0 to 35 mm, gas/particle velocities for three *w* are always larger than that in other position.

From *x*/*D*=0.1 to 1.5, the valley moves toward the wall. There is no valley for cross sections from *x*/*D*=1.5. For the four cross - sections 1.5<*x*/*D*<4.0, the peak values of the mean axial velocities begin decreasing. Until the last cross - section *x*/*D*=4.0, the distributions of the mean axial velocities are close to uniform. For all cross - sections, in the radial range 0<*r*<35mm, as the *w* increases, the value of the mean axial velocities increases. The reason is that as *w* increases, the quantity of gas/particle flow from inside to outside of the conical ring decreases and more gas/particle is gathered inside the conical ring.

4.2. Particle volume flux (By experiments)

Fig. 5 shows profiles of the axial particle volume flux for the three *w*. For each cross–section, in the radius range 35<*r*<70mm, the particle axial volume flux for the three *w* is low and increases as *x*/*D* increases. In each cross–section, within the radius range 0<*r*<35mm, the particle axial volume flux for the three *w* is always much greater than that in other radial positions, indicating that most of the gas/particle mixture exits from the third–level ring. In the four cross–sections from *x*/*D*=0.1 - 1.0, the peak values of the particle axial volume flux increase, as the *x*/*D* increases. With the development of the jet, the particle radial volume flux tends to become even. For the four cross - sections 0.1<*x*/*D*<1.0, the difference in the particle axial volume flux for the three *w* is not obvious. From Fig.4, it is known that in the radial range 0<*r*<35mm, with *w* increasing, the particle velocities get bigger and the inertia of particle increases, then the diffusion of particle is delayed. Therefore, for the four cross–sections from *x*/*D*=1.5 - 4.0, the peak of the particle axial volume flux increases as *w* increases obviously.

4.3. Influence of different w on the performance of concentration (By experiments)

Two parameters are defined to describe the concentration performance of the concentrator.

1). Rich/lean air ratio: R_Q

$$R_Q = 3 \times Q_r / Q_l \tag{3}$$

Where Q_r (m_3/s) is the air flux in the radius range from 0 to 35mm, Q_l (m_3/s) is the air flux in the radius range from 35 to 70mm.

Generally, R_Q is bigger than 1. The closer R_Q approaches 1, the more equal the distribution of the rich air velocity and lean air velocity. This can lead to even distribution of primary air flow and enhance the concentration performance.

2). Concentration ratio: R_C

$$R_C = C_r / C_l \tag{4}$$

C_r (kg/kg) is the pulverized coal concentration which is the ratio of pulverized coal quantity to air quantity in the radius range from 0 to 35mm, C_l (kg/kg) is the pulverized coal concentration in the radius range from 35 to 70mm.

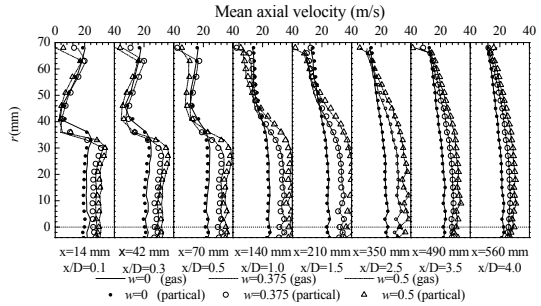

Figure 4. Profiles of the axial mean velocities for for different w

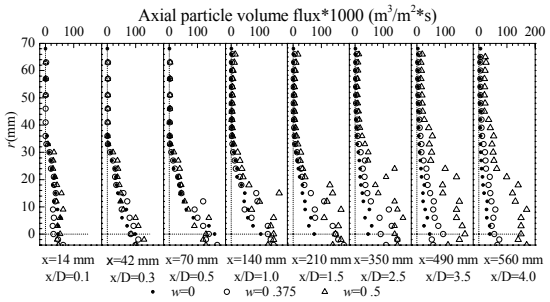

Figure 5. Profiles of the axial particle volume flux for different w

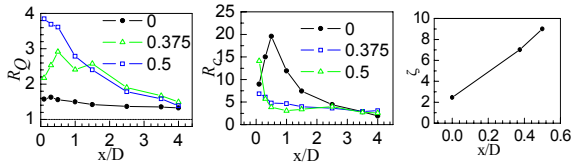

Figure 6. The distribution of RQ Rc and resistance coefficient (ζ) for different

The R_Q, R_c and resistance coefficient (ζ) of the three w were obtained and are given in Fig. 6. In each cross–section, R_Q of three w are always larger than 1.3. For cross-section x/D=0.1, R_Q for w=0.5 is 2.5 times of R_Q for w=0 and 1.9 times of R_Q for w=0.375. For cross-sections 0.1<x/D<1.5, as w increases, R_Q increases. For cross-sections 2.5<x/D<4.0, the difference of R_Q for w=0.5 and 0.375 is small. In each cross-section, R_Q for w=0 is smaller than for w=0.375 and 0.5. In each cross–section, R_C for each w is always larger than 2. For w=0.375 or 0.5, the peak value of R_C appears in the cross–section at x/D=0.1. For w=0, the peak value of R_C appears in the cross–section at x/D= 0.5. R_C then gradually decreases with x/D, which indicates that the distribution of the gas/particle mixture tends to gradually become even. However, the difference in R_C for the three w tends to become small as the value of x/D increases. In the cross–section at x/D=3.5, the influence of the w on R_C is minor. From Fig. 6, it is seen that the larger the w is, the larger ζ is. This can be explained by the fact that more of the gas/particle mixture passes through the exit of the third ring as w increases.

4.4. Verification of simulation

To validate the choice of grid divisions, the calculation model and methods, and the correctness of boundary conditions, a comparative study were performed. Fig. 7 graphs compared calculated mean axial velocities for the gas phase with experimental data in the outlet region for the case w=0. At the eight measurement cross–sections (x/D=0.1, 0.3, 0.5, 1.0, 1.5,

2.5, 3.5, and 4.0), these velocities were in good agreement, supporting the conclusion that the calculation model does describe the velocity field in the concentrator very well and confirms its applicability.

4.5. Particle trajectories, mean axial velocity contour and pathline (By calculation)

After flow though the conical ring, most of particles ejects from the outlet of the third – level ring (see Fig.8). For w=0, in the gap between the rings, part of particles flow from inside of the ring to outside. For w=0.2, 0.375 and 0.5, almost all particles ejects from the outlet of third – level ring. For the inertial effect, particles converge to the axis after a certain distance from the outlet of third – level ring, then diffusion to the wall. As w increases, the distance converged to the axis increases and diffusion is delayed. This is accordance with the experimental results of axial particle volume flux in Fig.5.

After the outlet of the third – level ring, in the radial range $0<r<35$mm, there is a high speed zone (see Fig.9). Compared to the inlet speed 16.7m/s, the axial velocity of the flow is significantly improved through the conical rings. As w increasing from 0 to 0.5, the length of the high speed zone along x direction increases. This is accordance with the experimental results in Fig.4. There is a recirculation zone outside each conical ring. As the level of ring increases, the size of recirculation zone increases. As the w increasing from 0 to 0.5, the size of the recirculation zone in same position increases. The existence of recirculation zone blocks the gas flow from inside of the ring to outside. For w=0.5, the gas flow from inside of rings to outside is little and the gas velocities near the wall is slow. Because of the driven of high speed gas flow in the central zone, a recirculation zone appears in certain distance after the outlet of the third – level ring. This restrains the diffusion of the gas flow.

4.6. Mean axial velocity within the conical ring region (By calculation)

Fig. 10 shows calculated radial profiles of the mean axial velocities of particles for twelve cross–sections within the conical ring region. Cross–section *before inlet* lies in the inlet region. Cross–sections *leading edge* 1, 2 and 3 correspond to the inlets of successive rings, cross – sections *middle* 1, 2 and 3 to midpoints and cross – sections *trailing edge* 1, 2 and 3 to outlets. The mean axial velocity values are maximal and uniform inside the conical ring. As w increases, the width of conical ring (b) increases and the diameter of the outlet of the first – and second – level ring decreases, so the radial range of the high speed zone decreases. As w increases, the quantities of gas flow from inside of ring to outside decreases, this result in R_Q increases. As w increases, the gas flux inside the ring increases and ζ increases. At the *leading* and *trailing edges* of the conical, mean axial velocities vanish. For cross–sections *leading edge* 1, 2 and 3, as w increases, the valley value of mean axial velocity decreases. For cross – sections *trailing edge* 1, 2 and 3, in the zone outside ring, the negative value range increases as w increases.

4.7. Mean radial velocity within the conical ring region (By calculation)

Fig. 11 shows calculated values of the mean radial velocities for concentrator region. In the vicinity of the axis and near the wall, the mean radial velocities vanish. These radial velocities obviously change near each leading edge trailing edges of a conical ring. As w increases, the width of conical ring (b) increases and the diameter of the outlet of the first – and second – level ring decreases, so the radial position of speed change point decreases. At the *leading edge* and *trailing edge* of the first–level ring, the mean radial velocities both have zero point. For *leading edge* 2 and 3, in the region between rings and axis, as w increases, the mean radial velocities decrease and in the region between rings and wall, the mean radial velocities decreases as w increases.

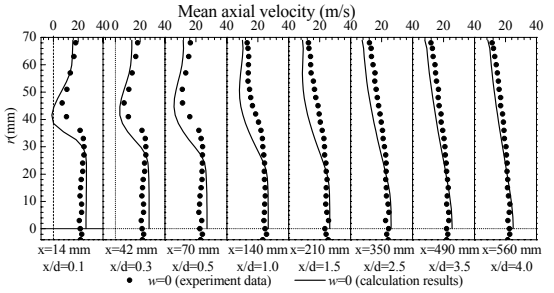

Figure 7. Comparison of calculated gas mean axial velocities with experimental data in the outlet region after the third–level ring for w=0.

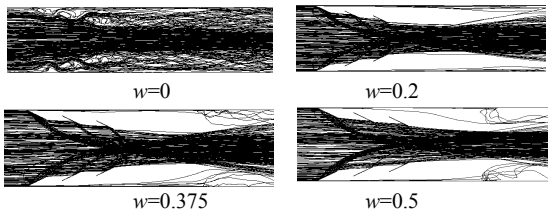

Figure 8. Calculated particle trajectories within a three–level conical ring for different w

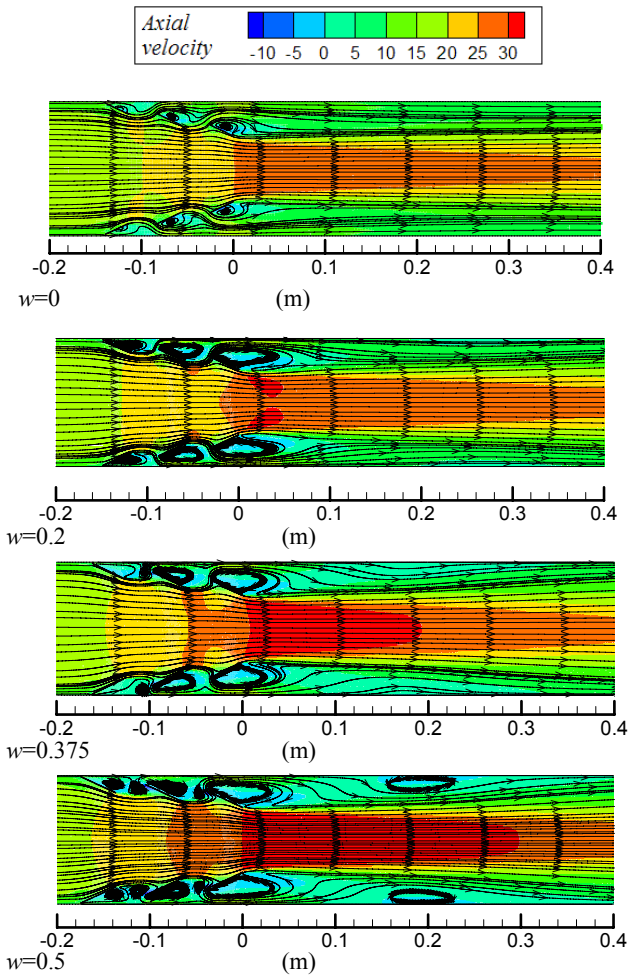

Figure 9. Calculated axial velocity contour and pathline within a three–level conical ring for different w

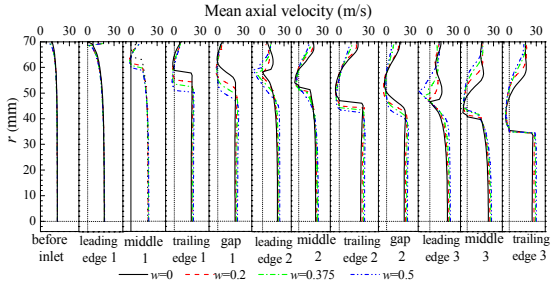

Figure 10. Calculated mean axial velocity profile within a three–level conical ring for different w.

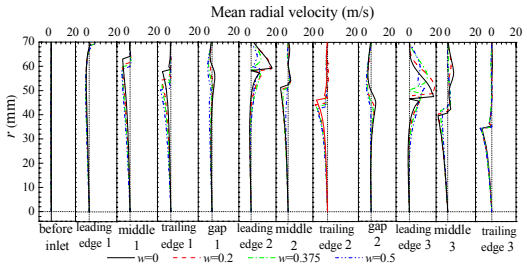

Figure 11. Calculated mean radial velocity profile within the conical ring region for different *w*

5. Conclusions

The influence of different cover ratio (*w*) on the gas/particle two–phase characteristics and resistance coefficient was obtained in this work. A PDA measurement system was employed in the study to measure after the outlet of third－level ring. And the numerical simulations were used to calculate the flow field in the conical ring region.

In each cross–section, R_Q of three *w* are always larger than 1.3 and R_c is always larger than 2. As *w* increases, R_c decreases in the cross-sections $0.5<x/D<3.5$ and ζ is increases. w=0 is the best case among w=0, 0.375 and 0.5.

In the outlet region, in the radial range $0<r<35$mm, the axial velocities and axial particle volume flux are bigger than that of other points in the same cross-section.

In the radial range $0<r<35$mm, as *w* increases, the mean axial velocities in the outlet region increase and uneven of gas distribution along radial direction increases. For w=0.5, almost all particles and gas ejects from outlet of the third－level ring.

In the conical ring region, as *w* increases, the size of recirculation zone outside the ring increases. For $w\geqslant0.375$, in the inlet position of the second－ and third－level ring, new recirculation zones appear. This result in gas flow from inside of the ring to outside further reduces and ζ increases.

6. Acknowledgments

This work was supported by the Hi–Tech Research and Development Program of China (Contract No. 2007AA05Z301), the Post–doctoral Startup Foundation of Heilongjiang Province and the Development Program for Outstanding Young Teachers in Harbin Institute of Technology.

References

[1] G. J. Liu, L. G. Zheng, L. F. Gao, H. Y. Zhang, Z. C. Peng. “The characterization of coal quality from the Jining coalfield,” Energy 2005, vol. 30(10) pp. 1903–1914.

[2] E. H. Chui, A. J. Majeski, M. A. Douglas, Y. Tan, K. V. Thambimuthu, "Numerical investigation of oxy-coal combustion to evaluate burner and combustor design concepts," Energy 2004, vol. 29(9-10) pp. 1285–1296.

[3] R. P. Lans, P. Glarborg, K. Dam-Johansen, "Influence of process parameters on nitrogen oxide formation in pulverized coal burners," Prog Energy Combust Sci 1997, vol. 23(4) pp. 349–371.

[4] L. B. Thomas, C. Francisco, C. Sebastien, P. Stanislas, B. Jacques, B. Bernard, "Coal combustion modelling of large power plant, for NOx abatement," Fuel 2007, 86(14): 2213-2220.

[5] P. Heil, D. Toporov, H. Stadler, S. Tschunko, M. Förster, R. Kneer, "Development of an oxycoal swirl burner operating at low O2 concentrations," Fuel 2009, vol. 88(7) pp. 1269–1274.

[6] National Standard of the People's Republic of China, GB13223-2003, Emission standard of air pollutants for thermal power plants 2004.

[7] H. Zhou, K. F. Cen. "Experimental measurements of a gas-solid jet downstream of a fuel-rich/lean burner with a collision-block-type concentrator," Powder Technology 2006, vol. 170 pp. 94–107.

[8] W. D. Fan, Y. Y. Li, Z. C. Lin, M. C. Zhang, "PDA research on a novel pulverized coal combustion technology for a large utility boiler," Energy 2010, vol. 35 pp. 2141-2148

[9] M. D. Horton, F. P. Goodson, L. D. Smoot. "Characteristics of flat, laminar coal-dust flames," Combust Flame 1977, vol. 28 pp. 187–195.

[10] J. M. Bee´r. "Combustion technology developments in power generation in response to environmental challenges," Progress in Energy and Combustion Science 2000, vol. 26 pp. 301–327.

[11] H. Zhou, K. F. Cen. "Experimental measurements of a gas-solid jet downstream of a fuel-rich/lean burner with a collision-block-type concentrator," Powder Technology 2006, vol. 170 pp. 94–107.

[12] X. L. Wei, T. M. Xu, S. E. Hui, "Burning low volatile fuel in tangentially fired furnaces with fuel rich/lean burners," Energy Conversion and Management 2004, vol. 45 pp. 725–735.

[13] Y. Zhang, L. X. Zhou, X. L. Wei, H. Z. Sheng, "Studies of the effect of a coal concentrator on NO formation in swirling coal combustion," International Journal of Heat and Mass Transfer 2006, vol. 49 pp. 421–426.

[14] Z. Q. Li, F. Wei, Y. Jin, "Numerical simulation of pulverized coal combustion and NO formation," Chemical Engineering Science 2003, vol. 58 pp. 5161–5171.

[15] W. D. Fan, J. H. Gao, Z. C. Lin, "Experiment and numerical simulation study about performance of louver pulverized coal concentrator [J] ," Power Engineering (2000), vol. 20 (5) pp. 831–838 (in Chinese).

[16] W. D. Fan, M. C. Zhang, J. H. Gao, "PDPA experimental study on gas-solid flow in louver concentrator [J] ," Journal of Combustion Science and Technology (2001), vol. 7 (3) pp. 214–218 (in Chinese).

[17] Z. Q. Li, Z. C. Chen, R. Sun, S. H. Wu, "New low NOx, low grade coal fired swirl stabilised technology," Journal of the Energy Institute 2007, vol. 80(3) pp. 123-130.

[18] Z. C. Chen, Z. Q. Li, J. P. Jing, L. Z. Chen, S. H. Wu and Y. Yao, "Study on flow fields of centrally fuel rich swirl burner and its applications," Korean journal of chemical engineering 2009, vol. 26(5), pp. 1186-1193.

[19] Z. C. Chen, Z. Q. Li, F. Q. Wang, J. P. Jing, L. Z. Chen, S. H. Wu, "Gas/particle flow characteristics of a centrally fuel rich swirl coal combustion burner," Fuel 2008, vol. 87(10-11) , pp. 2102-2110.

[20] Z. C. Chen, Z. Q. Li, F. Q. Wang, J. P. Jing, L. Z. Chen, S. H. Wu, Y. Yao, "Gas/particle flow characteristics of two swirl burners," Energy Conversion and Management 2009, vol. 50(5) , pp. 1180-1191.

[21] Z. Q. Li, J. P. Jing, Z. C. Chen, F. Ren, B. Xu, H. D. Wei, Z. H. Ge, "Combustion characteristics and NOx emissions of two kinds of swirl burners in a 300-MWe wall-fired pulverized-coal utility boiler," Combustion Science and Technology 2008, vol. 180(7) , pp. 1370-1394.

[22] Z. C. Chen, Z. Q. Li, J. P. Jing, F. Q. Wang, L. Z. Chen, S. H. Wu, "The influence of fuel bias in the primary air duct on the gas/particle flow characteristics near the swirl burner region," Fuel Processing Technology 2008, vol. 89(10) , pp. 958-965.

[23] T. H. Shih, W. W. Liou, A. Shabbir, Z. Yang and J. Zhu, Computers Fluids 1995, vol. 24(3) , pp.227–238.

[24] A. D. Gosman, E. Loannides, AIAA 19th Aerospace Science Meeting. Louis, Missouri; 1981.